Vacuum 184 (2021) 109924

Contents lists available at ScienceDirect

Vacuum

journal homepage: http://www.elsevier.com/locate/vacuum

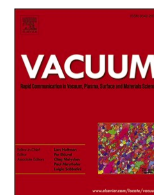

Vacuum refining of silicon at ultra-high temperatures

Arman Hoseinpur [a,b,*], Jafar Safarian [a,b]

[a] Department of Materials Science and Engineering, Norwegian University of Science and Technology (NTNU), Trondheim, Norway
[b] Norwegian Center for Sustainable Solar Cell Technology, Norway

ARTICLE INFO

Keywords:
Solar grade silicon (SoG-Si)
Vacuum
Evaporation
Phosphorus
Kinetics
Mechanisms

ABSTRACT

In the production of solar grade silicon (SoG-Si), Phosphorus (P) removal from Si is a challenge as it cannot be eliminated effectively by the final key directional solidification step in the value chain of the silicon solar cell technologies. The present research investigates the application of ultra-high temperatures (UHTs) up to 1900 °C for the P removal from Si in the vacuum-induction refining (VIR) process. Kinetic parameters such as mass transfer coefficient and activation energy for P removal from Si melt by vacuum evaporation are determined. It is shown that the P removal kinetics is significantly accelerated with increasing temperature, and about 1800 °C is a critical temperature in which the process rate is doubled. The silicon loss of the process to reach SoG-Si quality is formulated, and it is shown that it is lower at ultra-high temperatures, while it is insignificantly increased with the temperature rise in each temperature regime, and is independent of the melt geometry. The results from UHTs experiments showed complete phosphorus removal from silicon melts with even as high as P concentrations as 92.71 ppmw in short durations. It is shown that the application of UHTs in VIR process reduces the power consumption to reach SoG-Si.

1. Introduction

Power production by Photovoltaics is growing, and according to the sky scenario of shell® [1], 32% of the global power by the year 2070 could be generated by solar energy. Currently, about 90% of solar panels are produced from Silicon (Si) [2]. The Si used for the production of Si solar panels must have a purity of 99.9999 (6 N) known as solar grade silicon, shortly named as SoG-Si [3]. As the silicon produced in submerged arc furnaces from primary raw materials (MG-Si) has a purity of up to 99%, it needs to be refined to meet the SoG-Si requirements. Several metallurgical methods are recently introduced for the removal of impurities from Si, such as slag refining [4], leaching refining [5], plasma refining [6], solvent refining [7], gas refining [8,9], and vacuum refining [10–14]. Phosphorus (P) is so important to be controlled in Si since it is one of the major dopants for making the p-n junction in Si. Currently, 0.2 ppmw phosphorus could be considered as the acceptable limit of P in SoG-Si. Vacuum refining is a very efficient process for P removal from Si, and it is commercialized recently for the production of SoG-Si [15].

Phosphorus removal from Si by vacuum refining has been the subject of many researches since the early 1990s [10,16–23]. The thermochemistry and kinetics of P evaporation from Si melt have been studied. It is shown that the first-order reaction kinetic model fits well for studying the vacuum refining process [3,13,19,24–28]. The rate-controlling steps of the P evaporation from Si have been discussed before [19,29], and it has been shown that at temperatures up to 1700 °C the important steps are mainly evaporation from the melt surface, and diffusion through the gas phase. Theoretical models for the diffusion of P and other impurities in the melt, evaporation from melt surface, and diffusion through the gas phase were developed by Safarian and Tangstad in Ref. [13] and shown a good agreement between the analytical model and experimental data. These models have been later applied by Shi et al. in Ref. [21] to study their experimental results from a vacuum electron beam refining (EBR) furnace. Recently the effect of alloying of silicon by Al [14,22] and Fe [30] was investigated, indicating the acceleration in P removal rate in both of the cases compared with MG-Si refining.

The vacuum refining of P has been investigated in vacuum-induction refining (VIR) and EBR furnaces. The maximum temperature of 1700 °C was applied in the vacuum refining process of Si in the VIR furnace previously [13,31], while in the EBR higher temperatures, as high as 2247 °C are also reported [11,32]. In comparison, in EBR process the surface area of the melt pool could not be precisely determined, and there is a significant temperature gradient over the melt surface from the

* Corresponding author.
E-mail address: arman.h.kermani@ntnu.no (A. Hoseinpur).

https://doi.org/10.1016/j.vacuum.2020.109924
Received 13 October 2020; Received in revised form 16 November 2020; Accepted 17 November 2020
Available online 27 November 2020
0042-207X/© 2020 The Authors. Published by Elsevier Ltd. This is an open access article under the CC BY-NC-ND license (http://creativecommons.org/licenses/by-nc-nd/4.0/).

center to the round sides, and the bulk melt is colder than the surface due to the heat extraction by the water-cooled container. However, in the VIR process, the temperature is more homogeneous all over the bulk melt and can be measured directly by thermocouples. It is worth noting that, in EBR process direct temperature measurement is not possible, and the researchers estimated the average temperature of the melt-pool from the extent of Si evaporation [11]; the application of pyrometer is also recently reported [21]. Regarding the better control of process parameters in the VIR technique, this research deals with VIR application at ultra-high temperatures. Here we define ultra-high temperatures (UHT) as the temperatures higher than $1.25T_m$, where T_m is the melting point of silicon (T_m = 1414 °C), and therefore UHTs are higher than 1767 °C. This study is the first experimental work beyond this temperature carried out by VIR. The main objective of this research is to extract the kinetic data for the process and outline a proper understanding of temperature effect. Attempts are also made in this work to propose mechanisms for P removal at ultra-high temperatures. In addition, the vacuum refining of silicon in large scale needs to attain high enough mass transfer coefficients and we intend to show in this work that temperature rise is a key parameter to consider for improving the process rate.

2. Experimental procedure

In this research, a mixture of Silgrain® (HQ – micron cut; 0.04 wt% Fe, 0.09 wt% Al, 0.013 wt% Ca, 0.001 wt% Ti, 25 ppmw P, 30 ppmw B) and FBR® (8 N purity) silicon was used as the initial material for the P removal from Si melt. In most the experiments, Silgrain® (40–50 wt%) was mixed with FBR® granules, and then the mixture was charged into a dense graphite (Tanso®, properties presented in Ref. [33]) crucible. The experiments with some details about the practical conditions is listed in Table 1. In the experiment (E6) a master alloy of Si with P (314.1 ± 7 ppmw) was mixed with the FBR®. This master alloy was prepared by the addition of red phosphorus to Si as we elaborated [19]. The experiments at T ≤ 1750 °C were done in graphite crucibles with 70 mm inner diameter. Due to safety issues, it was decided to apply smaller crucibles (52 mm inner diameter) for experiments at higher temperatures, while the ratio of the melt surface area (A) over volume (V)was kept consistent in all the experiments ($A/V = 22.64\, m^{-1}$). We tried to measure the crucibles weight changes before and after experiment, however, in most of the cases the graphite crucibles burst because of silicon expansion during solidification. Then a part of the silicon melt was drained off and reacted with the graphite felt and therefore biased the final weight, preventing us to calculate the weight change. However, the crucibles of experiments E7 and E8 survived and we managed to measure the weight change of these crucibles after the VIR process. Considering the weight of Si samples taken from melt, 10 ± 0.1 g (4.65 wt% in 60 min) and 5 ± 0.1 (2.33 wt% in 25 min) grams of Si was lost in experiments E7 and E8, respectively. By dividing the measured amount of the silicon loss over melt surface area and time of the vacuum refining process, we calculated the experimental evaporation flux of silicon for the experiments E7 and E8 as 1.0278 and 1.7130 ($gm^{-2}s^{-1}$).

Table 1
The practical conditions in experiments.

Exp. Code	Temperature (°C)	Inner diameter of crucible (mm)	Initial Si mass (g)	Melt surface area[a] (mm^2)	Flux of Si loss ($gm^{-2}s^{-1}$)
E1	1500	70	400	3671.74	N. D.
E2	1600	70	400	3671.74	N. D.
E3	1650	70	400	3671.74	N. D.
E4	1750	70	400	3671.74	N. D.
E5	1850	70	400	3671.74	N. D.
E6	1800	52	215	1974	N. D.
E7	1850	52	215	1974	1.0278
E8	1900	52	215	1974	1.7130

[a] The occupied area by the graphite sheath (with 15 mm diameter) is subtracted from the inner cross area of the crucible for calculating the melt surface area, in all the experiments A/V = 22.64 m^{-1}, N. D: not determined, refer to experimental procedure section where the difficulties of wight loss measurements are mentioned.

The schematic representation of the vacuum-induction furnace applied in this research is presented in Fig. 1. The furnace is equipped with a mechanical pump with the pumping speed of 400 L min^{-1} over the pressure range of 1–30 Pa and the minimum pressure attainable was >7 Pa in the vacuum experiments. As shown, the graphite crucible is wrapped with a layer of graphite felt in a mica sheet, to be protected of contacting with the water – cooled copper coil. A thermocouple (T.C.) type C was used for measuring and recording the temperature in the melt during the experiments. The T.C. was put in a graphite well (15 mm outside diameter, tube with one end closed), fixed to the wall of the crucible.

After fixing the crucible in the induction coil, the chamber was vacuumed down to 5 Pa and subsequently filled out by Ar gas (5 N purity) up to 1000 mbar. This process was repeated three times to make sure that air left in the chamber is very rare. Then the heating was started and after melting the material, the first sample was taken from the melt, then the power was quickly increased to reach the target temperature (usually less than 1 min), while the chamber was continuously pumped. Several samples were taken from the melt at different time intervals to track the P concentration change during the VIR process. For sampling, a quartz tube (with 2 mm inner diameter and 6 mm outer diameter) was inserted into the middle of the melt and liquid silicon was sucked into the tube, then the tube was pulled out. The sampling time was short, below 30 s, and the thick quartz tube could tolerate both heat and the compressive forces due to the volume increase upon the Si sample solidification expansion. These Si samples were characterized by Induction coupled plasma mass spectroscopy (ICP – MS, Agilent – 8800 ICP-MS Triple Quad).

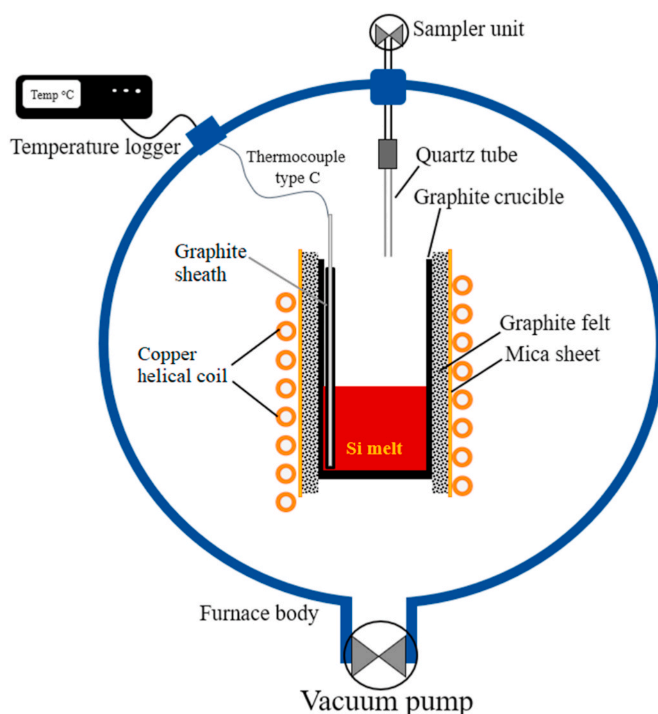

Fig. 1. Schematic representation of the VIR furnace and the set up with dedicated sampling unit.

3. Results and discussion

The results of P measurements from the vacuum refining experiments are all presented in Table 2. This table indicates that the P concentration is declining in all the experiments by the time and the refining rate is increased with increasing temperature. The preliminary results from the experiments done at UHTs (experiment E5) revealed the extremely faster rate of P removal than the lower temperatures. Thus, the time intervals for the vacuum refining steps were shortened at these experiments. Table 2 indicates that the last samples in all the experiments done at UHTs are almost free of phosphorus and below the detection limit of the ICP-MS. Even for the experiment E6, which initially contained 92.71 ppmw phosphorus, its P composition reached to the SoG-Si limit (0.2 ppmw) at 60 min of vacuum refining and it was free of P after 80 min of vacuum refining. This indicates the great efficiency of VIR process to remove any extent of phosphorus from the melt, which is more effective at higher temperatures. Considering the results of experiment E8 in Table 2, it is seen that only 25 min of vacuum refining was enough to remove all the initial 12.7 ppmw phosphorus from the melt.

Empirical kinetics and the mechanism of P removal from Si will be discussed in the following section (3.1). A discussion about required time for vacuum refining to reach SoG-Si and Si loss during the refining process will be presented in sections, 3.2 and 3.3 respectively. The power consumption in VIR process is presented in sections 3.4 followed by possible methods for implementation of the UHT-VIR in large scale in section 3.5.

3.1. Rate of P removal

The obtained experimental data presented in Table 2 are applied in this section to discuss the kinetics of VIR process. In order to find a right kinetic model which fits to our experimental data, we tried the first and second order kinetic models, and only the first order model fit well as previously observed [13]. The first order kinetic model could be introduced by below equation;

$$\ln\left(\frac{[\mathrm{P}\ \%]_0}{[\mathrm{P}\ \%]_t}\right) = k_\mathrm{P}\left(\frac{A}{V}\right)t \tag{1}$$

where $[\mathrm{P}\ \%]_0$ and $[\mathrm{P}\ \%]_t$ denote the initial and instant concentrations of phosphorus in the melt, respectively. the A/V ratio describes the geometry of the melt, where A and V are the surface area and volume of the melt in m^2 and m^3, respectively. Parameter k_P in equation (1) is called the mass transfer coefficient of phosphorus removal from silicon melt which is in $m\cdot s^{-1}$. By plotting the term $\ln([\mathrm{P}\ \%]_0/[\mathrm{P}\ \%]_t)$ versus the term (At/V) in the right side of equation (1), and fitting a line to the data, we can obtain the coefficient k_P, for each experiment, as it is illustrated in Fig. 2. The slopes of the fit lines represent the k_P values and they are given with the R-squared values in Fig. 2. The effect of the process temperature on the rate of P removal could be observed by comparing all the k_P values obtained in Fig. 2, where for instance k_P at 1900 °C is almost 52 times higher than the k_P at 1500 °C. Regarding the k_P values at various temperatures, we can determine the process kinetic parameters of the P evaporation from Si, like activation energy, by employing the Arrhenius [34] equation which is presented as follows;

$$k_\mathrm{P}\left[\mathrm{m}\cdot\mathrm{s}^{-1}\right] = k_\mathrm{P}^{*} exp\left(\frac{E_\mathrm{P}^{app}}{\mathrm{R}\ \ T}\right) \tag{2}$$

where k_P^* is a constant called Arrhenius pre-exponential factor, E_P^{app} is the apparent activation energy for the evaporation of P from Si and is in $\mathrm{J\cdot mol^{-1}}$, T denotes the absolute temperature in Kelvin (K), and R represents the universal gas constant (8.314 J $\mathrm{mol^{-1}\ K^{-1}}$). By plotting the

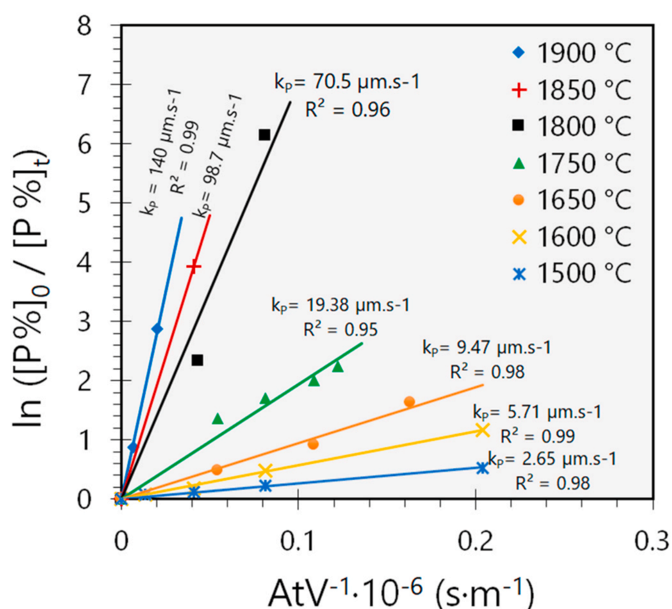

Fig. 2. First order reaction kinetic model fitting to the experimental data at various temperatures.

Table 2
The concentration of P (ppmw) in Si samples at various temperatures and times, measured by ICP – MS.

Time (minutes)	Experiments code and process temperature (°C)							
	E1	E2	E3	E4	E5	E6	E7	E8
	1500	1600	1650	1750	1850	1800	1850	1900
0	9.50	10.00	8.96	8.73	9.50	92.71	9.12	12.70
5								5.29
10	8.81	9.27						0.76
15								
25								<0.10[a]
30	8.84	8.40					0.18	
31						9.05		
40			5.55	2.24				
45					<0.10[a]			
55								
60	7.57	6.20		1.67		0.20	<0.10[a]	
80			3.50	1.17	<0.10[a]	<0.10[a]		
90				0.98				
150	5.58	3.10						
160			1.69					

a. Not detected in ICP-MS, where the detection limit was 0.10 ppmw

$\ln(k_P)$ values at various temperatures versus the reversed absolute temperature (T^{-1}) and fitting a line through the data, we can obtain the process E_P^{app} and k_P^* parameters, as shown in Fig. 3. As seen, all the data from the experiments below 1750 °C, are on the fit line with a high value of squared-R. This line will be shortly named LT (low temperature) fit line across this paper. Selected experimental data from the literature are also shown in Fig. 3. We can see those experiments that are done in almost over the same pressure range as of this study, are n good agreement with the LT while lower pressures [10,23] leads to increase of the mass transfer coeffects. It is noteworthy to mention that the research done by Safarian et al. [13,19] was done in the same furnace applied in this research, while Shi et al. [21] used an electron beam vacuum furnace for their study. Fig. 3 shows that the apparent mass transfer coefficient from the experiments at UHTs are much greater than the lower temperatures and they are not aligned with the extrapolation of the LT fit line. Therefore, another line is fit to the ultra-high temperature data with a high value of squared-R and is named hereafter UHT fit line. This observation is unique in the Arrhenius plot of P evaporation fromSi, and it has not been observed and reported elsewhere. The interesting point about the UHT fit line is that it has almost the same slope of the LT fit line, however it has just been displaced up in position, leading to cross the vertical axis at a higher point. The asterisk mark on Fig. 3 represents the mass transfer coefficient of P removal (with the value of 27.13 μm s^{-1}) expected to be obtained by extrapolation of the LT line at 1800 °C. Considering the k_P values presented on Fig. 3, it can be seen that the k_P at 1800 °C is 2.6 times greater than of the hypothetical value expected by the extrapolation of LT fit line. Table 3 represents the estimated apparent activation energy of phosphorus evaporation from Si (E_P^{app}) and the k_P^* calculated by both the LT and UHT fit lines as the results are given in Table 3.

In addition, it may be questioned if the $k_P$values of UHTs experiments, presented in Fig. 3, are affected by the crucibles size, since experiments E6 - E8 were carried out in smaller crucibles. To clarify this question, we need to compare experiment E5 with E7, which are both carried out at 1850 °C, but the former in big crucible and the latter one in small crucible. Considering Fig. 3, the LT and UHT fit lines predict the $k_{P@1850°C}$ to be 37.63 μm s^{-1} and 98.7 μm s^{-1}, respectively. Inserting both of these values into the first order kinetic model, equation (1), and considering 45 min for the time, it gives the phosphorus concertation 0.87 ppmw and 0.02 ppmw per k_P values from LT and UHT fit lines, respectively. However, Table 2 shows the phosphorus concertation of experiment E6 is less than 0.1 ppmw after 45 min (which is the detection limit of ICP-MS), and this indicates the k_P in experiment E5 is following the UHT line and therefore the phenomenon observed in Fig. 3 is independent of the crucible size and relates to the chemistry of the process.

Table 3
Determined kinetic parameters for the P evaporation from Si in vacuum induction refining.

Temperature range (°C)	E_P^{app} (kJ·mol^{-1})	$\ln(k_P^*, [\text{m}\cdot\text{s}^{-1}])$
T ≤ 1750	239.47	3.380
T ≥ 1800	256.84	5.337

3.1.1. Kinetic parameters

Here we will study the kinetic translation for the jump in k_P in Fig. 3 by reviewing the interpretation of the Arrhenius parameters in equation (2). We interpret these parameters in analogues to the reactions taking place in gases presented previously [35]. Fig. 4 represents the reaction coordinate defined as the collection of motions, such as changes in interatomic distances and bond angles, that are directly involved in the formation of products from the reactants. In the next section we will discuss the mechanisms of phosphorus evaporation and we will show that phosphorus can evaporate from silicon melt in various forms. Here, we take the simplest reaction for phosphorus evaporation from melt surface ($\underline{P} = P_{(g)}$) to discuss the mechanism of evaporation for phosphorus species as shown in Fig. 4. During the vacuum refining of Si, the dissolved $\underline{P}$ that already transferred to the melt surface forms an activated complex ($P \rightarrow P^*$). Having the maximum potential energy at the climax of the reaction coordinate, the phosphorus enters the transition state P^*. Here we shall preserve a distinction between the activated complex and transition state, the potential energy of the transition state is the maximum while it is close to the maximum for the activated complex. The activated complex represents the phosphorus atoms close to the maximum potential energy, but the transition state represents those atoms that are at the climax of the energy curve. Some molecules entering the transition state might revert to reactants, but those pass through this state convert to the product ($P^* \rightarrow P_{(g)}$), prior the gas

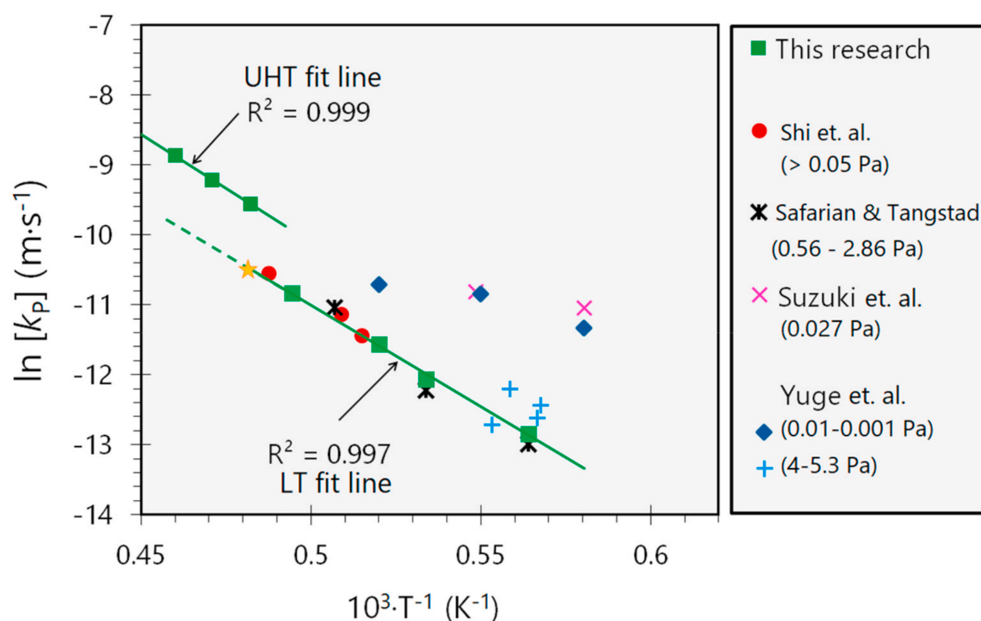

Fig. 3. Relationship between the mass transfer coefficient of P removal from Si and the reciprocal absolute temperature, data from literature Shi et al. [21], Safarian and Tangstad [13,19], Suzuki et. *al.* [23], *Yuge* et al. [10] *are included.*

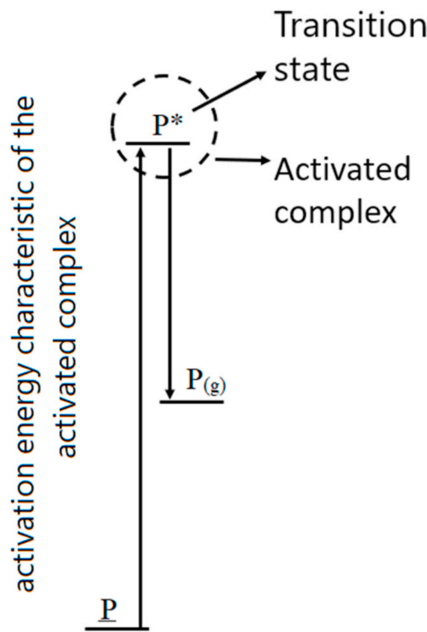

Fig. 4. The potential energy profile for the monoatomic phosphorus evaporation from Si melt introducing the activation energy, activated complex and transition state.

desorption. Therefore, the exponential term $\exp(-E_P^{app}/RT)$ in equation (2) is the fraction of the phosphorus species motions toward the appropriate positions for evaporation that have enough energy to lead the reaction. The pre-exponential factor is a measure of the rate of all motions of phosphorus toward forming activated complex irrespective of their energy. Therefore, the product of the k_P^* in equation (2) and the exponential factor $\exp(-E_P^{app}/RT)$ gives the rate of successful movements leading to form the transition state P^*.

As discussed above, if we consider a single reaction, the k_P^* corresponds to the rate of the formation of the activated complexes. Thus, the greater k_P^* represents the formation of more activated complexes at the melt surface. This may strike the idea that the sudden jump of k_P in Fig. 3 could be associated with the increase of the number of the activated complexes on the melt surface. However, the obtained k_P plotted in Fig. 3 are representing the whole VIR process and there could be several reactions leading to phosphorus removal. In next section we will discuss the possible mechanisms of phosphorus evaporation and show how they can affect the overall k_P.

3.1.2. Mechanisms of P evaporation

The main mechanism of P evaporation from Si is known to be by means of evaporation of monoatomic phosphorus ($P_{(g)}$) [13,19,31,36,37], however diatomic ($P_{2(g)}$) and tetratomic phosphorus ($P_{4(g)}$) are also mentioned in Refs. [31,36,38]. In this mechanism the phosphorus evaporates from melt surface by desorption in the form of $P_{(g)}$, $P_{2(g)}$, and $P_{4(g)}$. Here, we propose another mechanism to be involved by means of decomposition of silicon phosphides (SiP and SiP_2) transitionally formed

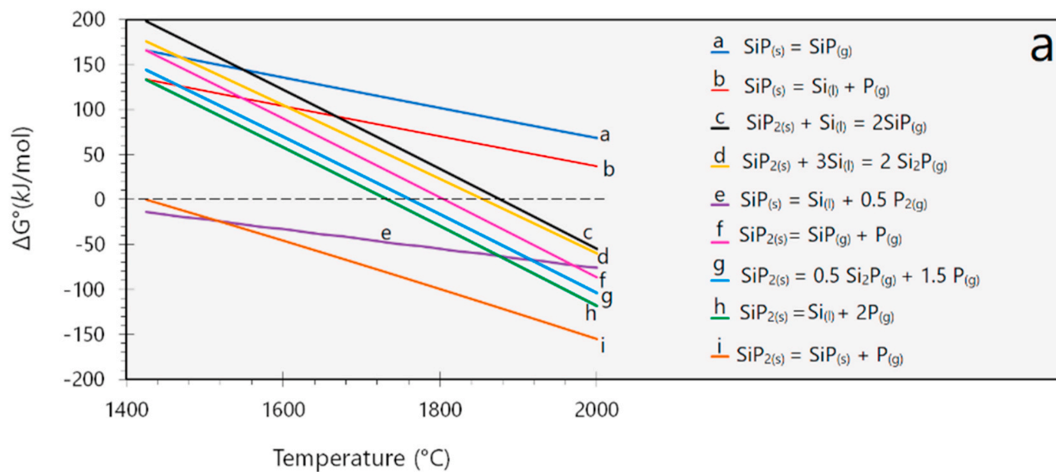

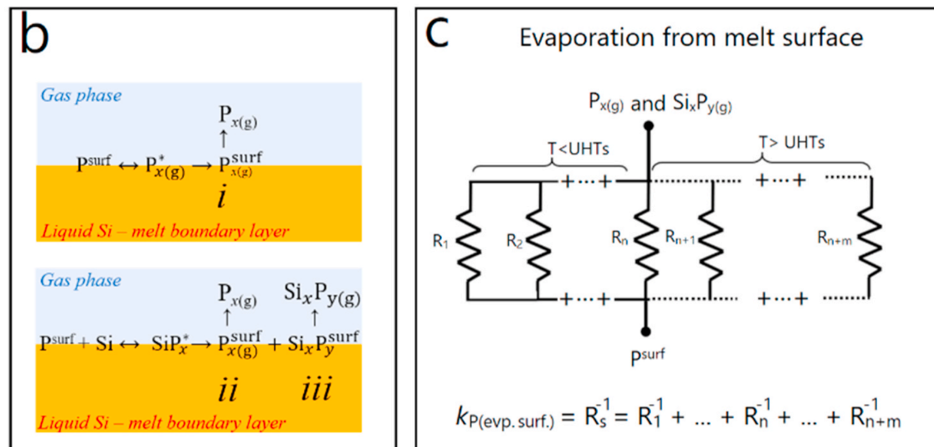

Fig. 5. The changes of the Gibbs energy of decomposition of phosphides, per mole of condensed phosphide (a), the proposed mechanisms for P evaporation from Si melt surface (b), and the electrical analogy for resistances to mass transfer and the routes for phosphorus to the gas phase at LT and UHT regimes (c).

on melt surface. Fig. 5(a) shows the standard Gibbs energy change for various decomposition paths of SiP and SiP_2 calculated by the thermodynamics software HSC 10 [39]. It is of worth to mention that the surface of liquid metals is in higher levels of energy than bulk liquid due to the incomplete coordination among the surface atoms [40]. This makes the phosphorus to be adsorbed more at the liquid metal surface which could lead to the formation of transitional SiP and SiP_2 molecules in short range orders. The presence of the SiP and SiP_2 in Si–P system is already discussed by Liang and Schmid-Fetzer [28]. The phase diagrams presented in Ref. [28] indicate that there is no silicon phosphide in the infinitely diluted solutions of P in Si. However, this does not invalidate the hypothesis of transient silicon phosphides formation at the melt surface since the system is not at equilibrium and P atoms may be more concentrated at the surface. These molecules could decompose, eventually leading to releasing of phosphorus gases ($P_{(g)}$, $P_{2(g)}$, and $P_{4(g)}$). A series of possible reactions scenarios for the decomposition of the SiP and SiP_2 are presented in Fig. 5(a). This figure shows that decomposition SiP_2 and SiP (reactions e and i) have negative values of ΔG° at elevated temperatures. However, the chemical reactions (c, d, f, g, h) have positive values of ΔG° changing to negative values by increasing the temperature over the range of 1725 °C–1875 °C, which yield $P_{(g)}$ or $Si_xP_{y(g)}$, and according to Fig. 5(a), there are more thermally activated feasible reactions when temperatures approaches to 1800 °C, which could explain the boost up of k_P observed about this temperature in Fig. 3.

Fig. 5(b) shows the possible scenarios of P evaporation from Si melt, which we propose to take place for phosphorus removal in VIR process at UHT. Totally, all the reactions leading to evaporation of phosphorus from Si melt could be categorized in three scenarios as follows;

i. Desorption of phosphorus gases: the phosphorus evaporation could take place by means of desorption of phosphorus gases ($P_{(g)}$, $P_{2(g)}$, and $P_{4(g)}$) from melt surface as shown in Fig. 5(b-*i*).
ii. Evaporation of phosphorus gases produced by decomposition of silicon phosphides: the evaporation of phosphorus gases ($P_{(g)}$, $P_{2(g)}$, and $P_{4(g)}$) by means of decomposition of the transient silicon phosphides (SiP and SiP_2) forming on the melt surface, as shown in Fig. 5 (b-*ii*).
iii. Evaporation of silicon phosphides: Phosphorus evaporation from melt surface in the form of silicon phosphides $Si_xP_{y(g)}$ as shown in Fig. 5 (b-*iii*).

In the first scenario, phosphorus in the melt boundary layer needs to reach to the melt surface (P^{surf}) and then form the activated complex (P_x^*, $x = 1$ or 2 or 4). Having enough energy, the P_x^* will transform to gaseous phosphorus, which is still adsorbed on the surface ($P^{surf}_{x(g)}$). Subsequently the $P^{surf}_{x(g)}$ desorbs from surface to form gaseous phosphorus ($P^{surf}_{x(g)} \rightarrow P_{x(g)}$). This mechanism describes the evaporation of phosphorus and is mentioned already in the literature [13,31]. However, Fig. 5(b-*ii*) suggests the second scenario for monatomic evaporation thorough the instant formation of SiP^* or SiP_2^* on melt surface. In this mechanism, the P^{surf} could interact with adjacent Si atoms to form SiP^* or SiP_2^*, which can subsequently transform to Si^{surf} or $Si_xP^{surf}_{y(g)}$ and $P^{surf}_{x(g)}$, and it is followed by $P^{surf}_{x(g)} \rightarrow P_{x(g)}$ as the last step of the above mechanism. Here it is noted that SiP_x^* is a transition state for SiP_x evaporation. The $Si_xP^{surf}_{y(g)}$ compounds could also evaporate directly, providing the third mechanism mentioned above (Fig. 5-b).

As we discussed above, three families of mechanisms could participate in phosphorus evaporation from silicon melt and each of them could take place through several reactions. Since all the above P evaporation mechanisms could take place parallelly on the melt surface, the total mass transfer coefficient for phosphorus evaporation from melt surface could be calculated from the equivalent circuit presented in Fig. 5(c). Considering the electrical analogy in Fig. 5(c), at low temperature regimes, there are fewer routs for phosphorus evaporation. Each of this routes (resistances) shown on the circuit represents a reaction leading to phosphorus evaporation. The low temperature active resistances for phosphorus evaporation (like R_1 and R_2) become smaller at UHTs regime and in parallel other routes that are only active at UHTs take part in the process. The change of ΔG° for chemical reactions (c, d, f, g, h) shown in Fig. 5(a) from positive to negative values is the thermodynamic evidence supporting this idea. The phosphorus mass transfer coefficient for evaporation from melt surface, $k_{P(surf)}$, is actually the reversed of the surface resistance (where R_s overall surface resistance) as shown on Fig. 5(c)), and it becomes smaller significantly at UHTs.

Table 3 showed the process activation energy (E_P^{app}) slightly changes (about 7.22%) at UHTs which could be due to the phosphorus removal by the parallel mechanisms introduced in Fig. 5. We have to indicate E_P^{app} is the overall activation energy of the VIR process and is the result of all the phosphorus evaporation reactions. Fig. 5 shows a part of the phosphorus evaporation could be by means of SiP_2 decomposition. However, at UHTs the SiP_2 could find more routs to decompose, leading to increase in the $k_{P(surf)}$, which is aligned with the significant increase of k_P at UHTs.

3.2. Required process time to obtain SoG-Si

Now that the kinetic parameters for phosphorus removal from silicon melt are obtained, we can calculate the minimum time that is required to do the VIR process to reach the silicon with the phosphorus concentration that is acceptable for SoG-Si production. For this purpose, we just need to insert the calculated k_P values obtained for each temperature into the first order kinetic model presented in equation (1) and consider the acceptable limit of phosphorus concertation in SoG-Si as the final phosphorus concertation. Then the time to be calculated by equation (1), will be the required time of doing vacuum refining to reach SoG-Si at each temperature. Here, we start by rewriting equation (2) in terms of time as follows;

$$t_{SoG-Si}[\text{hours}] = \frac{1}{3600 \frac{A}{V} k_P} \ln\left(\frac{[P\%]_0}{[P\%]_{SoG-Si}}\right) \quad (3)$$

where the t_{SoG-Si} denotes the required time of the vacuum refining (in hours) to reach SoG-Si, and $[P\%]_{SoG-Si}$ is the maximum acceptable concentration of phosphorus in Si for solar applications, assumed to be $[P\%]_{SoG-Si} = 0.2$ ppmw in this paper. The t_{SoG-Si} for melts containing various initial concentrations of phosphorus, from 5 ppmw to 100 ppmw, are calculated and presented in Fig. 6. This figure indicates the

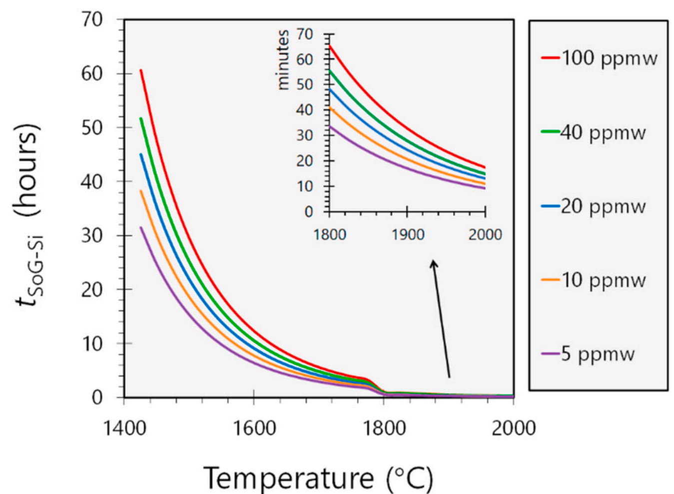

Fig. 6. The required time to obtain SoG-Si (t_{SoG-Si}) *over temperature calculated for various melts with different initial phosphorus concertation.*

impact of temperature on shortening the required time to do the vacuum refining. As it is shown in Fig. 6, the t_{SoG-Si} for melt with $[P\%]_0 = 5\,ppmw$ reduces from 30 h to half an hour by increasing the process temperature from 1425 °C to 1800 °C, which is 60 times faster and of practical importance. Fig. 6 show a rapid decline at 1800 °C. This is due to the sudden increase in the k_P, shown in Fig. 3. The inset plot in Fig. 6 represents a magnification of the t_{SoG-Si} curves at ultra-high temperatures (T ≥ 1800 °C). Comparing the t_{SoG-Si} curves containing 5 ppmw and 100 ppmw of initial phosphorus, it can be seen that these curves approach each other at higher temperatures indicating that the refining time for different melts with various initial contents of phosphorus is almost similar at ultra-high temperatures. The difference in t_{SoG-Si} for refining of the melts with 100 ppmw and 5 ppmw is 30 h at 1425 °C, while it is around 30 min at 1800 °C for the both initial compositions, and much shorter at higher temperatures. This indicates the significant role of the temperature in the VIR of Si and could be of interest for industrial application as at higher temperatures the required time for the process goes independent of the initial P concentration. In other words, higher temperatures make the process almost independent of the raw material quality and hence make the process robust to the various sources of raw materials.

3.3. Si loss in VIR process

The Si evaporation during the vacuum refining can be calculated by the theoretical evaporation formula of Hertz – Knudsen – Langmuir (HKL), presented as follows;

$$J_{Si}^{HKL}\left[\frac{g}{m^2 s}\right] = \alpha \ p^{\circ}Si\sqrt{\frac{M_{Si}}{2\pi RT}} \tag{4}$$

where the J_{Si}^{HKL} denotes the maximum theoretical mass flux of Si evaporation, α is the accommodation coefficient (we assume it unity for

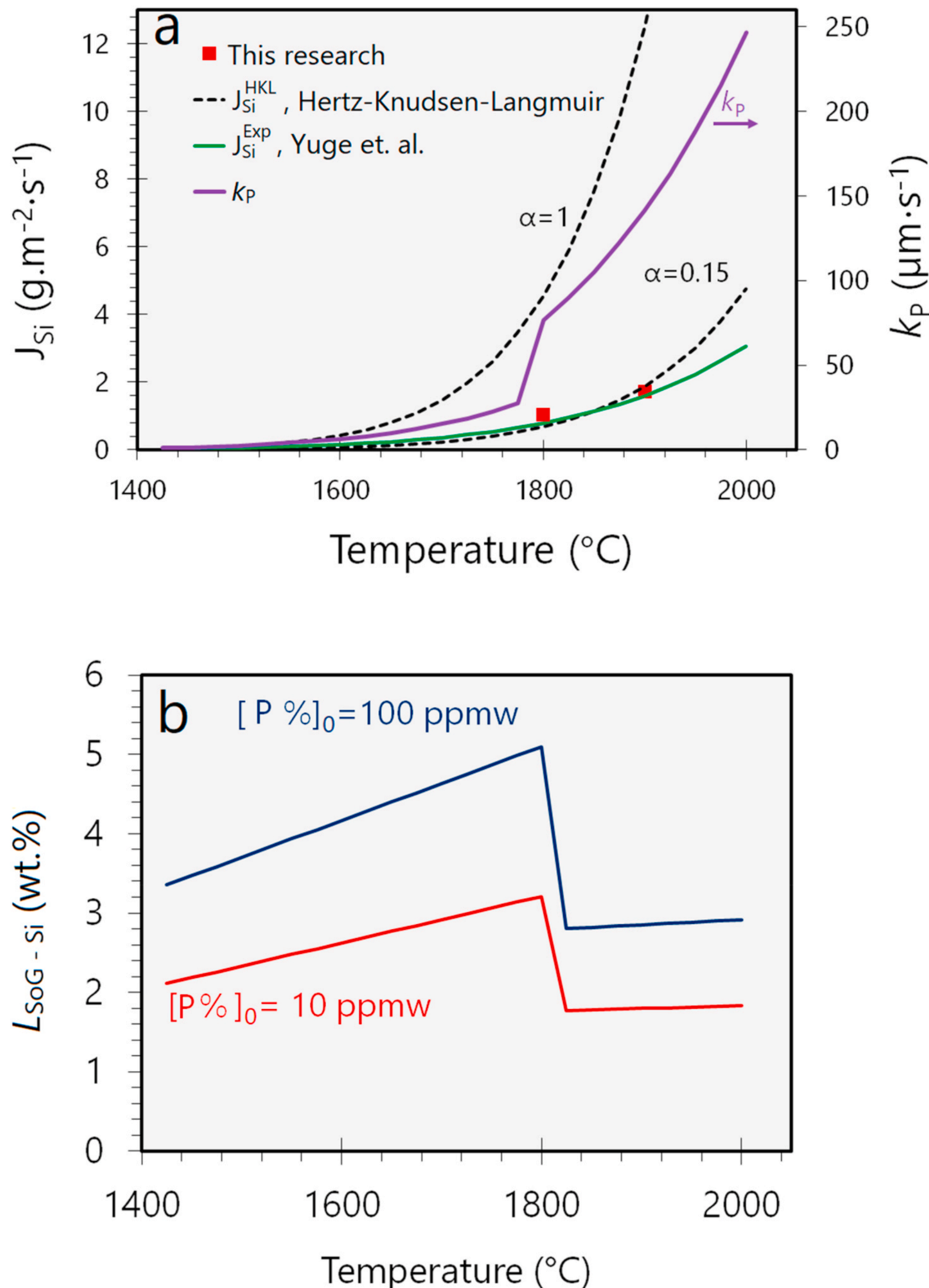

Fig. 7. (a): The flux of Si evaporation and apparent mass transfer coefficient of P in VIR process as a function of temperature. (b): the L_{SoG-Si} *over various temperatures.*

perfect conditions), p°_{Si} is the saturated vapor pressure of Si, ($\log p^{\circ}_{Si}$ [Pa] $= (-20900 \cdot T^{-1}) - 0.565 \log T + 12.905$ [41]), and M_{Si} is the molar mass of Si. Equation (4) presents the simplest form of HKL equation for a perfect vacuum condition, and hence the Si re-condensation to melt surface is assumed to be ignorable. More details about Hertz – Knudsen equation could be found in Ref. [42]. Thus, equation (4) gives the maximum evaporation flux of Si from melt surface. An empirical formula for Si evaporation has been presented by Yuge et al. [10], based on the experiments carried out in VIR furnace and graphite crucible and over the temperature range of 1450 °C–1650 °C, as given here:

$$J^{Exp}_{Si}\left[\frac{g}{m^2 s}\right] = 1000 \exp\left(8.29 - \frac{32000}{T}\right) \tag{5}$$

where the J^{Exp}_{Si} denotes the flux of Si evaporation. Applying equations (4) and (5), the flux of Si evaporation as a function of temperature is calculated as it is illustrated in Fig. 7(a). The apparent mass transfer coefficient of phosphorus (k_P) and the experimental data of Si loss (in 1800 and 1900 °C) are also shown in Fig. 7(a). This figure shows that the empirical formula for silicon evaporation developed by Yuge et al. [10] is in good agreement with the Si mass loss in our VIR experiments. Now, having the Si evaporation flux in hand and applying the following equation one can calculate the weight percent of the silicon loss during the experiments as follows;

$$L_{Si}[wt.\%] = \frac{J_{Si}At}{m_{Si,0}}.100 \tag{6}$$

where the L_{Si} denotes the silicon loss in experiment until time t, and $m_{Si,0}$ denotes the initial mass of the Si melt. Now, for calculating the amount of Si that is lost until reaching the SoG-Si (assumed to be Si with 0.2 ppmw phosphorus), we need to insert the t_{SoG-Si} into equation (6), which gives:

$$L_{SoG-Si}[wt.\%] = \frac{100\, J_{Si}}{k_P \rho_{Si}} ln\left(\frac{[P\%]_0}{[P\%]_{SoG-Si}}\right) \tag{7}$$

where L_{SoG-Si} denotes the Si loss in the vacuum refining process associated with the required time to do the vacuum refining for reaching SoG-Si, and ρ_{Si} is the density of Si melt that ($2.5 \cdot 10^6$ g m^{-3}). Equation (7) unveils an important feature of the vacuum refining of silicon; it shows that the L_{SoG-Si} is independent of the crucible shape (A/V), and the initial mass of the melt. Now by inserting the experimental evaporation flux of silicon (equation (5)) and k_P (equation (2)) into equation (7) we can obtain the following formula to calculate the L_{SoG-Si} in wt.%:

$$L_{SoG-Si}[wt.\%] = \begin{cases} 0.04\ \ ln\left(\frac{[P\%]_0}{[P\%]_{SoG-Si}}\right)\exp\left(4.9 - \frac{3916}{T}\right), & T < 1800\,^{\circ}C \\ 0.04\ \ ln\left(\frac{[P\%]_0}{[P\%]_{SoG-Si}}\right)\exp\left(2.95 - \frac{1107}{T}\right), & T \geq 1800\,^{\circ}C \end{cases} \tag{8}$$

This equation is applied to calculate the L_{SoG-Si} and the result is shown on Fig. 7(b). It is obvious from Fig. 7(b) that the L_{SoG-Si} increases by process temperature until 1800 °C and then suddenly drops at this temperature, due to the sudden increase in k_P already shown on Fig. 3. Fig. 7(b) also shows beyond 1800 °C, the L_{SoG-Si} does not change so much with temperature.

It is worth mentioning that equation (8) is independent of melt surface area and volume; therefore, it only depends on the initial P concentration. In other words, equation (8) could be applied to any melt geometry and crucible shape. The information presented by Figs. 6 and 7 (b) indicates that the vacuum refining at ultra-high temperatures is of great benefit to make use of the advantages of shorter process time and less silicon loss. Fig. 6 also indicates the minimum L_{SoG-Si} is at 1800 °C, where the k_P has a sudden increase making it a unique temperature in the vacuum refining of the Si melt.

3.4. Theoretical power consumption in VIR process

As the significant effect of UHTs on vacuum evaporation of P from Si were shown in the previous sections, it is important to study the effect of UHTs on power consumption of the process. Hence, this section deals with theoretical power consumption of VIR process at various temperatures. The total energy required for VIR process P_{req}, could be presented as:

$$P_{req}[kWh] = Q_1 + \Delta H_{fusion} + Q_2 + \left(Q_{cond} + Q_{rad} + Q_{evp}\right)_{loss} \tag{9}$$

where P_{req} includes the energy for heating Si from room temperature to its melting point (Q_1), the fusion enthalpy (ΔH_{fusion}), the excess heat for increasing the temperature from melting point to the VIR temperature (Q_2), and the heat loss during the VIR process. Three forms of heat loss could be assumed for the VIR process, as presented in the parentheses in equation (9), where,Q_{cond} and Q_{rad} are heat losses by conduction (via crucible wall) and radiation from the surface, respectively. Parameter Q_{evp} is heat loss due to evaporation from the surface. Applying the FactSage® 7.3 software [43], the Q_1, $\Delta H_{fusion}$are calculated as 3.553×10^{-4} kWhg^{-1} and 4.968×10^{-4} kWhg^{-1}, respectively and Q_2 is a function of temperature (regarding the superheat to UHT) as follows;

$$Q_2 = 1.08 \cdot 10^{-4}\ T - 0.018\ (kWh\,/\,g) \tag{10}$$

Assuming a perfect insulation of the crucible, negligible loss by conduction, the theoretical heat loss in VIR process could be presented by the following equation:

$$Q_{rad}[kWh] = q_{rad} t_{SoG-Si} \tag{11}$$

$$Q_{evp}[kWh] = q_{evp} t_{SoG-Si} \tag{12}$$

where t_{SoG-Si} is the time of VIR process in hour, q_{rad} and q_{evp} denote the heat flows (W) by radiation and mass transfer due to Si evaporation, respectively. The q_{rad} can obviously be determined by the Stefan-Boltzmann law;

$$q_{rad}\ [W] = A\varepsilon\sigma T^4 \tag{13}$$

where ε is the emissivity of Si melt equal to 0.21 [44] and σ is the Stefan-Boltzmann constant with the value of 5.67×10^{-8} (Wm^{-2}K^{-4}). In dilute solutions of P in Si, the mean loss will be due to Si evaporation since impurities have much low concentration. Therefore, rate of the heat loss by mass evaporation from surface could also be calculated by means of the following equations;

$$q_{evp}\ [W] = J_{Si}\ A\ \Delta H_{evp} \tag{14}$$

$$\Delta H_{evp}\left[Jg^{-1}\right] = -0.1897T + 14319 \tag{15}$$

where $\Delta H_{evp}$is the evaporation enthalpy of Si over the range of melting point to 2273 K (calculated by FactSage® 7.3 [43]). Inserting the theoretical evaporation flux of silicon J^{HKL}_{Si} into equation (14), the heat loss by mass evaporation could be calculated. Fig. 8(a) represents the calculated heat flow per unit area for evaporation and radiation as a function of temperature, which are called the evaporation heat flux ($\dot{q}_{evp}$) and the radiation heat flux ($\dot{q}_{rad}$), respectively. Fig. 8(a) shows that both $\dot{q}_{rad}$ and $\dot{q}_{evp}$ are increased by the operating temperature of VIR process, and temperature has greater effect on heat loss by evaporation compared to radiation. The radiation from melt surface is the main mechanism of heat loss from T_m up to 2125 °C where $\dot{q}_{evp}$ exceeds the $\dot{q}_{rad}$, making the evaporation the major mechanism of heat loss beyond tis temperature. The total flux of heat loss from melt surface, $\dot{q}_{surf}$, could be obtained by the summation of $\dot{q}_{rad}$ to $\dot{q}_{evp}$, as it is shown in Fig. 8(a) and can be calculated as a function of temperature thorough the

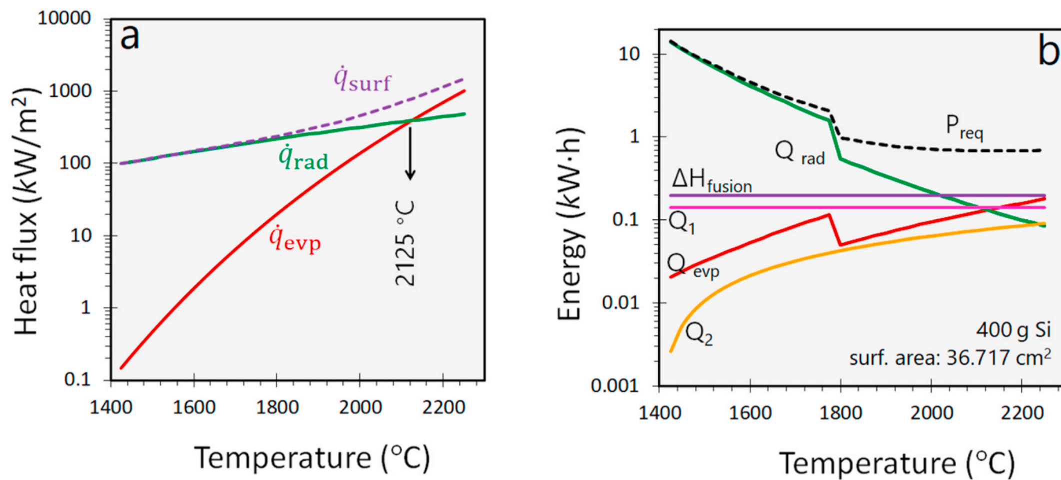

Fig. 8. (a) The fluxes of heat loss by radiation and silicon evaporation. (b) required power and the other energy supply/losses for vacuum refining process to get SoG-Si, calculated for a melt with 10 ppmw phosphorus. (For interpretation of the references to colour in this figure legend, the reader is referred to the Web version of this article.)

following equation:

$$\dot{q}_{surf}\left[kWm^{-2}\right] = 9\times10^{-9}\cdot T^{4} - 9\times10^{-5}\cdot T^{3} + 0.1452\cdot T^{3} - 161.56\cdot T + 67309 \quad (16)$$

As the flux of heat loss is obtained, we can calculate the corresponding required power to do the vacuum refining for obtaining SoG-Si. Fig. 8(b) represents the relationship between energy consumption by the above-mentioned mechanisms and the total required power, P_{req}, and the applied process temperature. This figure indicates that the Q_{evp} and Q_2 increase by the process temperature, while the Q_{rad} reduces. This figure shows clearly the impact of Q_{rad} is greater than the other parameters and it controls the P_{req} up to 1800 °C, and its sharp drop at UHT is leading to significant reduction of P_{req}. Therefore, UHT vacuum refining also is very beneficial for reduction of power consumption to obtain SoG-Si.

3.5. Implementation of UHT-VIR process

The most important challenge in vacuum refining of silicon at moderate temperatures is the process rate as the mass transfer coefficient is not high enough and the process implementation must be done with increasing the melt surface area per unit volume. In the previous sections we showed that the UHT-VIR process for Si refining provides very large mass transfer coefficients and so from technical point of view there is no need to provide large surface to volume ratio. Moreover, the UHT process shortens the refining time, reduces the Si loss, and even the overall energy consumption. We propose here possible methods to implement the UHT-VIR in large scale.

Although different technologies can be applied to do the UHT-VIR process, we show two viable technologies as schematically presented in Fig. 9. One technology is like the applied lab method in this study and literature [13,17,19,45] in which the whole volume of the melt is heated and stirred by electromagnetic forces, or other techniques. And the other technology is this volume heating (by induction or resistance techniques) in combination with a surface heating technique. Several

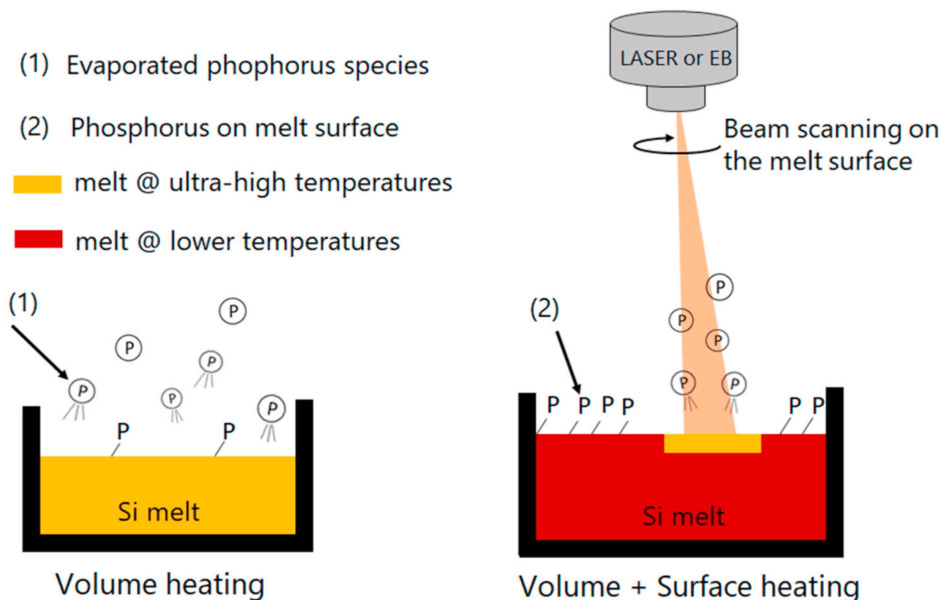

Fig. 9. Two typical proposed methods for implementation the VIR in large scale.

techniques could be candidates for the surface heating such as pancake induction coils, laser beam heating, electron beam heating (etc.) techniques. The second technique has the advantage of providing high-speed process, while the melt bulk is in lower temperature, which is more suitable for the refractories, furnace lifetime, and even lower energy consumption (for heating the bulk melt). Fig. 9 depicts the surface heating by laser technique while the melt bulk is kept in lower temperatures. As shown schematically, when the laser beam scans the melt surface, the temperature increases to UHTs locally at the shedding point, leading to evaporation of the phosphorus already present melt surface. In the combined method, having the melt bulk well stirred by induction, the phosphorus diffusion in melt will not be the rate controlling step. As shown in Fig. 8 the major part of the power consumption is Q_{rad} and thus surface heating will not help to energy efficiency of the process compared to the volume heating technique.

4. Conclusions

We have studied the P removal from Si by ultra-high temperature vacuum refining method for SoG-Si production. Empirical kinetics of P removal from Si, mechanisms of P evaporation, Si loss during the VIR, required power consumption, and methods for implementation of the UHT-VIR were discussed. It has been summarized as follows:

i. Effective complete removal of P from Si is feasible at ultra-high temperatures, starting from certain concentrations of P in Si.
ii. The overall mass transfer of P removal from silicon melt increases by temperature rise, and there is a sudden increase at the temperature about 1800 °C.
iii. Mechanisms for P removal at UHT was proposed in which the gasification of P from the dominant monoatomic (at lower temperatures) is changed to both monoatomic evaporation, and evaporation by means of silicon phosphides formation at the surface followed by their decomposition/evaporation.
iv. It was shown L_{SoG-Si} increases by temperature and suddenly drops at 1800 °C due to the sudden increase in k_P.
v. The temperature 1800 °C can be an optimum temperature for VIR since regarding the lowest Si loss, high rate of phosphorus removal, low power consumption.

Declaration of competing interest

The authors declare that they have no known competing financial interests or personal relationships that could have appeared to influence the work reported in this paper.

Acknowledgments

This research was financed by Norwegian University of Science and Technology (NTNU) and was done in cooperation with the Research Center for Sustainable Solar Cell Technology (FME SuSolTech) in Norway. The support from Elkem® Bremanger for silicon material is highly acknowledged.

References

[1] Shell Scenarios Shell, Sky - Meeting the Goals of the Paris Agreement, 2018, p. 72. https://www.shell.com/energy-and-innovation/the-energy-future/scenarios/shell-scenario-sky.html.
[2] D.S. Philips, W. Warmuth, Photovoltaics Report, Fraunhofer ISE, 2016, pp. 1–43, https://doi.org/10.1016/j.compedu.2008.05.004.
[3] X. Lu, T. Miki, O. Takeda, H. Zhu, T. Nagasaka, Thermodynamic criteria of the end-of-life silicon wafers refining for closing the recycling loop of photovoltaic panels, Sci. Technol. Adv. Mater. 20 (2019) 813–825, https://doi.org/10.1080/14686996.2019.1641429.
[4] H. Chen, K. Morita, X. Ma, Z. Chen, Y. Wang, Boron removal for solar-grade silicon production by metallurgical route:A review, Sol. Energy Mater. Sol. Cells 203 (2019) 110169, https://doi.org/10.1016/j.solmat.2019.110169.
[5] M. Zhu, A. Azarov, E. Monakhov, K. Tang, J. Safarian, Phosphorus separation from metallurgical-grade silicon by magnesium alloying and acid leaching, Separ. Purif. Technol. 240 (2020), https://doi.org/10.1016/j.seppur.2020.116614.
[6] C. Alemany, C. Trassy, B. Pateyron, K.-I. Li, Y. Delannoy, Refining of metallurgical-grade silicon by inductive plasma, Sol. Energy Mater. Sol. Cells 72 (2002) 41–48, https://doi.org/10.1016/S0927-0248(01)00148-9.
[7] K. Morita, T. Yoshikawa, Thermodynamic evaluation of new metallurgical refining processes for SOG-silicon production, Trans. Nonferrous Met. Soc. China (English Ed. 21 (2011) 685–690, https://doi.org/10.1016/S1003-6326(11)60766-8.
[8] Ø.S. Sortland, M. Tangstad, Boron removal from silicon melts by H2O/H2 gas Blowing : mass transfer in gas and melt, Metall. Mater. Trans. E. 1 (2014) 211–225, https://doi.org/10.1007/s40553-014-0021-x.
[9] M. Vadon, Ø. Sortland, M. Tangstad, G. Chichignoud, Y. Delannoy, Passivation threshold for the oxidation of liquid silicon and thermodynamic Non-equilibrium in the gas phase, Metall. Mater. Trans. B 49 (2018) 3330–3342, https://doi.org/10.1007/s11663-018-1381-x.
[10] N. Yuge, K. Hanazawa, K. Nishikawa, H. Terashima, Removal of phosphorus , aluminum and calcium by evaporation in molten silicon, J. Jpn. Inst. Metals 61 (1997) 1086–1093.
[11] T. Ikeda, M. Maeda, Purification of metallurgical silicon for solar-grade silicon by electron beam button melting, ISIJ Int. 32 (1992) 635–642, https://doi.org/10.2355/isijinternational.32.635.
[12] K. Hanazawa, N. Yuge, S. Hiwasa, Y. Kato, Evaporation of phosphorus in molten silicon with electron beam irradiation method, Mater. Trans. 45 (2004) 844–849.
[13] J. Safarian, M. Tangstad, Vacuum refining of molten silicon, Metall. Mater. Trans. B 43 (2012) 1427–1445, https://doi.org/10.1007/s11663-012-9728-1.
[14] A. Hoseinpur, J. Safarian, Phosphorus removal from Al-doped silicon by vacuum refining, in: 35th Eur. Photovolt. Sol. Energy Conf. Exhib. Phosphorus, Bruxel (2018) 469–472, https://doi.org/10.4229/35thEUPVSEC20182018.
[15] Ceccaroli Forniés, Souto Méndez, Pérez Vázquez, Dieguez Vlasenko, Mass production test of solar cells and modules made of 100% UMG silicon. 20.76% record efficiency, Energies 12 (2019) 1495, https://doi.org/10.3390/en12081495.
[16] N. Yuge, M. Abe, K. Hanazawa, H. Baba, N. Nakamura, Y. Kato, Y. Sakaguchi, S. Hiwasa, F. Aratani, Purification of metallurgical-grade silicon up to solar grade, Prog. Photovoltaics Res. Appl. 9 (2001) 203–209, https://doi.org/10.1002/pip.372.
[17] S.S. Zheng, W.H. Chen, J. Cai, J.T. Li, C. Chen, X.T. Luo, Mass transfer of phosphorus in silicon melts under vacuum induction refining, Metall. Mater. Trans. B Process Metall. Mater. Process. Sci. 41 (2010) 1268–1273, https://doi.org/10.1007/s11663-010-9422-0.
[18] T. Kemmotsu, T. Nagai, M. Maeda, Removal rate of phosphorus from molten silicon, High Temp. Mater. Process. 30 (2011) 17–22, https://doi.org/10.1515/htmp.2011.002.
[19] J. Safarian, M. Tangstad, Kinetics and mechanism of phosphorus removal from silicon in vacuum induction refining, High Temp. Mater. Process. 31 (2012) 73–81, https://doi.org/10.1515/htmp.2011.143.
[20] K. Wei, D. Zheng, W. Ma, B. Yang, Y. Dai, Study on Al removal from MG-Si by vacuum refining, Siliconindia 7 (2015) 269–274, https://doi.org/10.1007/s12633-014-9228-9.
[21] S. Shi, P. Li, J. Meng, D. Jiang, Y. Tan, H.M.N. ul H.K. Asghar, Kinetics of volatile impurity removal from silicon by electron beam melting for photovoltaic applications, Phys. Chem. Chem. Phys. 19 (2017) 28424–28433, https://doi.org/10.1039/C7CP05080A.
[22] A. Hoseinpur, K. Tang, J. Safarian, Kinetic study of vacuum evaporation of elements from ternary melts; case of dilute solution of P in Si-Al melts, Separ. Purif. Technol. 235 (2020) 116284, https://doi.org/10.1016/j.seppur.2019.116284.
[23] K. Suzuki, K. Sakaguchi, T. Nakagiri, N. Sano, Gaseous removal of P and B from molten Si, J. Jpn. Inst. Metals 54 (1990) 161–167.
[24] X. Lu, T. Miki, T. Hiraki, H. Zhu, T. Nagasaka, Thermodynamics of elements in dilute silicon melts, JOM (J. Occup. Med.) 71 (2019) 1456–1470, https://doi.org/10.1007/s11837-019-03378-y.
[25] S. Favre, I. Nuta, G. Chichignoud, K. Zaïdat, C. Chatillon, Removing phosphorus from molten silicon: a thermodynamic evaluation of distillation, ECS J. Solid State Sci. Technol. 5 (2016) P129–P137, https://doi.org/10.1149/2.0361602jss.
[26] A.I. Zaitsev, A.D. Litvina, N.E. Shelkova, Thermodynamic properties of Si-P melts, High Temp. 39 (2001) 227–232, https://doi.org/10.1023/A:1017570715796.
[27] T. Miki, K. Morita, N. Sano, Thermodynamics of phosphorus in molten silicon, Metall. Mater. Trans. B 27 (1996) 937–941.
[28] S.-M. Liang, R. Schmid-Fetzer, Modeling of thermodynamic properties and phase equilibria of the Si-P system, J. Phase Equilibria Diffus. 35 (2014) 24–35, https://doi.org/10.1007/s11669-013-0269-3.
[29] S. Shi, W. Dong, X. Peng, D. Jiang, Y. Tan, Evaporation and removal mechanism of phosphorus from the surface of silicon melt during electron beam melting, Appl. Surf. Sci. 266 (2013) 344–349, https://doi.org/10.1016/j.apsusc.2012.12.022.
[30] J. Safarian, K. Tang, K. Hildal, Vacuum treatment of ferrosilicon, Sustain. Ind. Process. SUMMIT (2015) 261–268, 2015.
[31] S.S. Zheng, T. Abel Engh, M. Tangstad, X.T. Luo, Separation of Phosphorus from silicon by induction vacuum refining, Separ. Purif. Technol. 82 (2011) 128–137, https://doi.org/10.1016/j.seppur.2011.09.001.
[32] H. Sasaki, Y. Kobashi, T. Nagai, M. Maeda, Application of electron beam melting to the removal of phosphorus from silicon: toward production of solar-grade silicon by metallurgical processes, Ann. Mater. Sci. Eng. (2013) 1–8, https://doi.org/10.1155/2013/857196.
[33] A. Hoseinpur, J. Safarian, Mechanisms of graphite crucible degradation in contact with Si–Al melts at high temperatures and vacuum conditions, Vacuum 171 (2020) 108993, https://doi.org/10.1016/j.vacuum.2019.108993.

[34] S.K. Upadhyay, Chemical Kinetics and Reaction Dynamics, Springer Netherlands, Dordrecht, 2006, https://doi.org/10.1007/978-1-4020-4547-9.
[35] P. Atkins, J. Paula, Physical Chemistry, eighth ed., WH freman and company, Newyork, 2006.
[36] S.S. Zheng, T. Abel Engh, M. Tangstad, X.T. Luo, Numerical simulation of phosphorus removal from silicon by induction vacuum refinin, Metall. Mater. Trans. 42 (2011) 128–137.
[37] N. Yuge, H. Baba, Y. Sakaguchi, K. Nishikawa, H. Terashima, F. Aratani, Purification of metallurgical silicon up to solar grade, Sol. Energy Mater. Sol. Cells 34 (1994) 243–250, https://doi.org/10.1016/0927-0248(94)90046-9.
[38] S. Zheng, J. Safarian, S. Seok, S. Kim, T. Merete, X. Luo, Elimination of phosphorus vaporizing from molten silicon at finite reduced pressure, Trans. Nonferrous Metals Soc. China 21 (2011) 697–702, https://doi.org/10.1016/S1003-6326(11)60768-1.
[39] HSC Chemistry 10, http://www.hsc-chemistry.net/index.html.
[40] T. Iida, R.I.L. Guthrie, The Thermophysical Properties of Metallic Liquids, first ed., Oxford University Press, New York, 2015 https://doi.org/10.1093/acprof:oso/9780198729839.001.0001.
[41] O. Kubachewski, C.B. Alcock, Metallurgical Thermochemistry, fifth ed., Pergamon press ltd, NewYork, 1979.
[42] T. Ytrehus, S. Østmo, Kinetic theory approach to interphase processes, Int. J. Multiphas. Flow 22 (1996) 133–155, https://doi.org/10.1016/0301-9322(95)00056-9.
[43] factsage software version 7.3, www.factsage.com.
[44] E. Takasuka, E. Tokizaki, K. Terashima, S. Kimura, Emissivity of liquid silicon in visible and infrared regions, J. Appl. Phys. 81 (1997) 6384–6389, https://doi.org/10.1063/1.364418.
[45] J. Safarian, B.S. Xakalashe, M. Tangstad, Vacuum removal of the impurities from different silicon melts, Eur. Photovolt. Sol. Energy Conf. Exhib. Vac. (2011) 1810–1813, https://doi.org/10.4229/26thEUPVSEC2011-2BV.4.3.